# Improved Geoid Modeling Using Observed and Modeled Gravity Gradients in Taiwan

Yu-Shen Hsiao<sup>1</sup>; Cheinway Hwang<sup>2</sup>; Meng-Ling Wu<sup>3</sup>; and Jung-Chieh Chang<sup>4</sup>

Abstract: The authors present a new geoid modeling procedure that can greatly improve relative geoid accuracy in mountainous areas, leading to improved applications for modern geodetic techniques, such as light detection and ranging (LIDAR), in mapping orthometric heights over steep terrain on which precise slopes are needed to assess the risk of landslides and the suitability of industrial development. The new procedure (1) measures gravity gradients or computing modeled gravity gradients from a regular grid of gravity anomalies, (2) uses these gradients to refine gravity anomalies, and (3) uses the gravity anomalies to compute geoidal undulations. This new procedure was tested in Taiwan. In situ gravity gradients were measured at approximately 4,000 gravity sites to compare the modeled gravity gradients. In the test, ground gravity observations are reduced to gravity anomalies at mean sea surface using three types of gravity gradients: normal, modeled, and observed. The researchers' geoid modeling uses the method of least-squares collocation (LSC) with the remove-compute-restore (RCR) procedure. Free-air gravity anomalies, as reduced using the observed and modeled gravity gradients, deviate from those using normal gradients by up to 100 mgal in high mountains. Using free-air gravity anomalies derived from observed and modeled gravity gradients, the authors can improve the relative geoid accuracies by up to 17 and 18 cm, respectively, for Route 3 (an area with high mountains) in Taiwan. DOI: 10.1061/(ASCE)SU.1943-5428.0000212. © 2016 American Society of Civil Engineers.

Author keywords: Gravity; Geoid; Gravity gradients.

#### Introduction

Deriving an accurate geoid model over complex topography is challenging. One place with a rough topography is Taiwan, which was created by the collision of the Eurasian Plate and the Philippine Sea Plate. The collision of the two plates has resulted in undulating foothills and high mountains on the island of Taiwan and oceanic trenches, ridges, and basins in the Pacific Ocean east of Taiwan. Fig. 1(a) shows the free-air gravity anomalies obtained from landbased, shipborne, and airborne gravity measurements, as well as satellite altimetry (Hwang et al. 2014). The gravity field in Fig. 1(a) is highly correlated with the terrain and represents the most up-todate and comprehensive gravity field for the island of Taiwan and its surrounding seas. The gravity field has been used to determine a geoid model of Taiwan with accuracies ranging from the centimeter scale in plains to the decimeter scale in high mountains (Hwang et al. 2013). For modern geodetic techniques, such as airborne LIDAR, which has a decimeter-scale accuracy in measured heights (Hodgson and Bresnahan 2004), a geoid model with an equivalent accuracy is important for the techniques to derive useful orthometric heights. Decimeter-scale orthometric heights are also important

Note. This manuscript was submitted on February 19, 2016; approved on August 10, 2016; published online on October 5, 2016. Discussion period open until March 5, 2017; separate discussions must be submitted for individual papers. This paper is part of the *Journal of Surveying Engineering*, © ASCE, ISSN 0733-9453.

for assessing the risk of landslides and the suitability of residential construction, both of which are primarily based on the slope of the terrain.

Typically, ground gravity measurements are reduced to gravity anomalies using the normal gradient of -0.3086 mgal/m (Heiskanen and Moritz 1967). If the true gradient deviates from this normal value, errors in the gravity anomalies based on this value will be proportional to the elevation. As such, use of the normal gradient can lead to large errors in modeled geoidal undulations in high mountains, hindering techniques, such as LIDAR, from mapping decimeter-level orthometric heights.

There are a number of studies on the modeling and application of gravity gradients. Rapp and Pavlis (1990) used a second-order normal gradient to improve gravity reduction with elevation. Rozsa and Toth (2003) predicted gravity gradients using gravity and elevation data in Sóskút, Hungary. Tenzer and Ellmann (2007) used a mean gravity gradient for gravity reduction in the Canadian Rocky Mountains. Zhu and Jekeli (2009) combined airborne gradiometric data, ground gravity anomaly data, and a digital elevation model to model a gravity gradient field in Parkfield, California. Vanicek et al. (2000) used downward continuation to determine a mean gravity gradient, which was subsequently applied to geoid modeling in the Rocky Mountains. Furthermore, Völgyesi (2001) computed a geoid model in Cegléd, Hungary, using gravity gradient data. These studies conclude that the use of modeled gradients, instead of the normal gradient, can improve gravity field modeling. In these studies, the modeled gravity gradients were not validated by in situ gravity gradient measurements, and there is no investigation of the model improvement due to the use of nonnormal gravity gradients in connection to elevation. From 2006 to 2010, new land-based gravity values were measured at approximately 4,000 sites on the island of Taiwan and its offshore islands. The gravity gradients were also measured at the gravity sites. Although the new gravity values have contributed to a high-resolution gravity grid in Taiwan (Hwang et al. 2014), the gradient measurements have not been used to aid

<sup>&</sup>lt;sup>1</sup>Assistant Professor, Dept. of Soil and Water Conservation, National Chung Hsing Univ., 250 Guoguang Rd., Taichung 402, Taiwan (corresponding author). E-mail: yshsiao@nchu.edu.tw; geo.yshsiao@gmail.com

<sup>&</sup>lt;sup>2</sup>Chair Professor, Dept. of Civil Engineering, National Chiao Tung Univ., 1001 Ta Hsueh Rd., Hsinchu 300, Taiwan.

<sup>&</sup>lt;sup>3</sup>Graduate Student, Dept. of Civil Engineering, National Chiao Tung Univ., 1001 Ta Hsueh Rd., Hsinchu 300, Taiwan.

<sup>&</sup>lt;sup>4</sup>Graduate Student, Dept. of Soil and Water Conservation, National Chung Hsing Univ., 250 Guoguang Rd., Taichung 402, Taiwan.

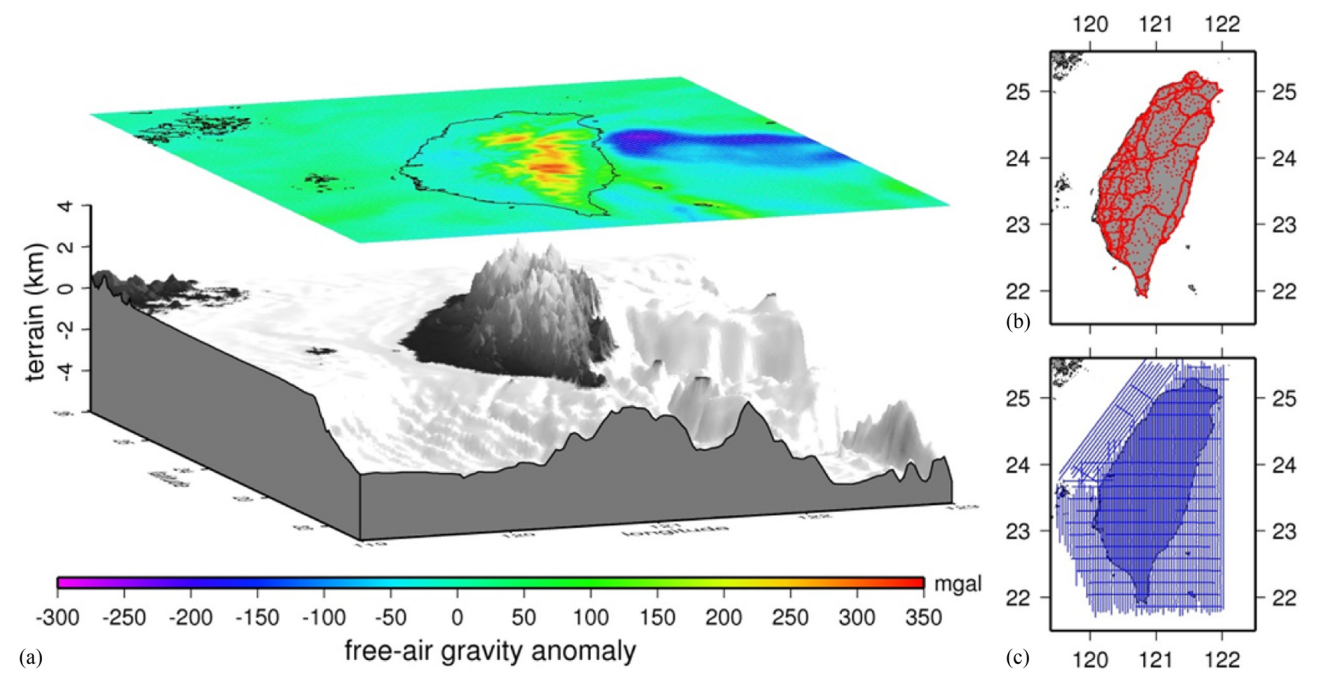


**Fig. 1.** (Color) (a) Free-air gravity anomaly (data from Hwang et al. 2014) and terrain; (b) earlier land-based gravity data; (c) airborne gravity data over Taiwan (Note: Neither the earlier land-based nor the airborne gravity estimates were used for good modeling in this study)

geoid modeling or to assess gradients that are based on models. In this study, the authors compute modeled gravity gradients and explore the potential of newly observed gradient measurements in improved gravity reduction and geoid modeling. Specifically, the deviations of the normal gradient (-0.3086 mgal/m) from the observed or modeled gradients in terms of height and location will be investigated. The gravity and geoid results from the observed and modeled gravity gradients will be compared with those based on the normal gradient. Depending on the availability of observed gravity gradients, the authors propose a new procedure of geoid modeling that can greatly improve relative geoid accuracy in high mountains.

In this paper, the authors do not model the second-order effect in gravity reduction or discuss the role of the normal gradient in the Molodensky method of geoid modeling. Instead, the authors emphasize the use of observed gravity gradients to improve geoid model accuracy in a method that has been used in previous works (Forsberg and Sideris 1993; Hwang et al. 2007).

## **Gravity Gradients in Taiwan: Observed and Modeled**

# **Gravity Gradients from Observations**

From 2006 to 2010, relative gravity measurements were made at approximately 4,000 gravity sites (the red dots in Fig. 2) in Taiwan using Graviton-EG relative gravimeters (LaCoste & Romberg, Inc., Austin, Texas). The temporal effects of solid earth tide, ocean tide, pressure change, and polar motion were removed from the raw gravity measurements. By fixing the absolute gravity values at 10 sites, the researchers performed a rigorous network adjustment (Hwang et al. 2002) to determine the gravity values at all 4,000 sites. The network adjustment yields an averaged standard deviation of 0.035 mgal for the adjusted point gravity values. Each gravity site was marked with a pillar, and three gravity readings at 0.0, 0.5, and 1.5 m above the pillar were made using a tripod-held plate. The sample photos in Fig. 2

show the different types of tripod-held plates used in the fieldwork. The researchers then computed the differences between the gravity values at the three different heights, resulting in three gravity gradients. The final gravity gradient for the site is the mean of the three gravity gradients. A gravity gradient was computed as

$$t = \frac{g_1 - g_2}{\Lambda h} \tag{1}$$

where  $g_1$  and  $g_2$  are gravity readings at different heights above the pillar; and  $\Delta h$  = height difference. According to error propagation, the accuracy of the gravity gradient  $\sigma_t$  is

$$\sigma_t = \sqrt{2} \frac{\sigma_g}{\Delta h} \tag{2}$$

where  $\sigma_g$  = resolution of the Graviton-EG gravimeter, which is 1  $\mu$ gal (Hwang et al. 2010). If  $\Delta h = 1$  m,  $\sigma_t = 0.0014$  mgal/m, which is the typical accuracy of the observed gravity gradient. When performing absolute gravity measurements at a site, such gravity gradients are also used in reducing absolute gravity values from a point above the pillar (typically associated with the instrument height) to the pillar.

### Modeled Gravity Gradients from Gravity Anomalies by Integration

In addition to the observed gradients, the authors also modeled gravity gradients as follows. If  $g_P$  is the observed gravity value at Point P on the ground, the corresponding value  $g'_P$  on the geoid can be computed (Heiskanen and Moritz 1967)

$$g_P' = g_P - \left(\frac{\partial g}{\partial H}\right) H_P \tag{3}$$

where  $H_P$  = orthometric height at P; and  $\partial g/\partial H$  = actual gravity gradient. The term  $\partial g/\partial H$  can be split into the normal gravity

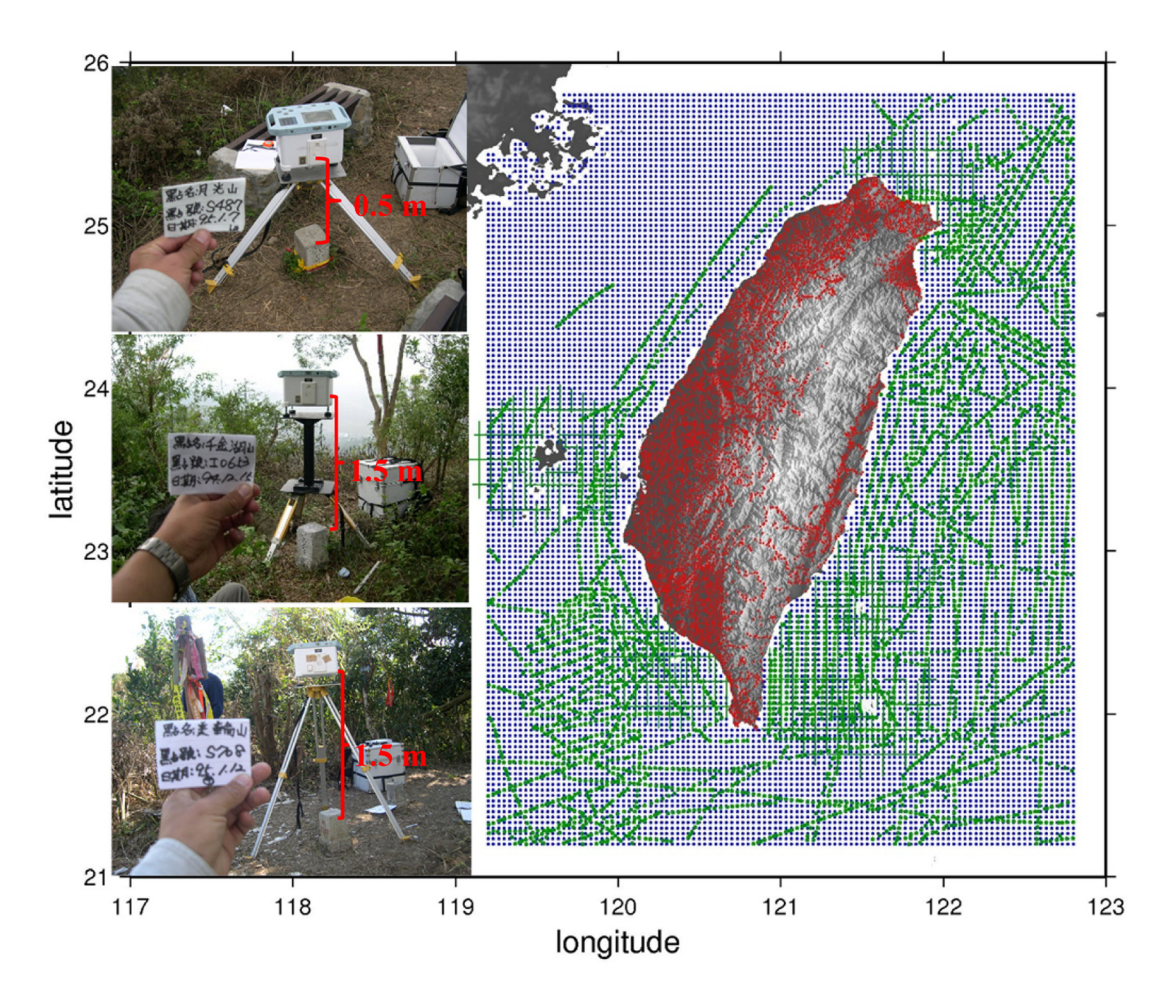


Fig. 2. (Color) Distributions of new land-based gravity data (red), altimeter-derived gravity data of Sandwell V23.1 (blue), and shipborne gravity data from NOAA and NLSC (green); the photographs show how a gravity gradient is observed by measuring gravity values with a tripod

gradient  $\partial \gamma / \partial h$  and the gravity anomaly gradient  $\partial \Delta g / \partial h$  (Heiskanen and Moritz 1967). As such, Eq. (3) can be expressed as

$$g_P' = g_P - \left(\frac{\partial \gamma}{\partial H} + \frac{\partial \Delta g}{\partial H}\right) H_P$$
 (4)

The term  $\partial \Delta g/\partial H$  at *P* is called the modeled gravity anomaly gradient and can be computed by (Heiskanen and Moritz 1967)

$$\frac{\partial \Delta g_P}{\partial H} = \frac{R^2}{2\pi} \iint_{\sigma} \frac{\Delta g - \Delta g_P}{l_0^3} d\sigma - \frac{2}{R} \Delta g_P \tag{5}$$

where  $\Delta g_P$  = gravity anomaly at P;  $\Delta g$  = gravity anomaly on the unit sphere; R = Earth's mean radius;  $l_0$  = spatial distance between P and the variable unit;  $l_0$  =  $2R \sin \psi/2$ ;  $\psi$  = angular distance;  $\sigma$  = unit sphere; and  $d\sigma$  = differential element of the area. Hwang and Hsiao (2003) proposed a method to compute  $\partial \Delta g_P/\partial H$  by the Gaussian quadrature integration (Gerald and Wheatley 1994) for the purpose of rigorous orthometric corrections. In this paper, the authors used the Gaussian quadrature method of Hwang and Hsiao (2003) to compute modeled gravity gradients on a regular grid in Taiwan using gravity anomalies from Hwang et al. (2014).

#### Assessing Modeled Gravity Gradients by Observations

In previous sections, the authors described the observed and modeled gravity gradients in Taiwan. Fig. 3 compares the observed gravity gradients and the modeled gravity gradients. Histograms were inserted in Fig. 3 to show the distributions of the kinds of gravity gradients and the differences between them. The statistics of the gradients are summarized in Table 1. Relatively large gravity gradients (absolute values) occurred in high mountains with the maximum gradient reaching -0.34 mgal/m. Gravity gradients in the western plains of Taiwan are smaller, ranging from -0.30 to -0.32 mgal/m (areas shaded by green and blue in Fig. 3). The observed gravity gradients and modeled gravity gradients, and the difference between the two, have standard deviations of 0.0057, 0.0085, and 0.0070, respectively, and mean values of -0.3115, -0.3078, and -0.0050 mgal/ m, respectively. The overall magnitude of the observed gradients (absolute values) is larger than that of the modeled gradients. The range of modeled gradients is larger than that of observed gradients. Fig. 4 shows the correlation between the observed and modeled gravity gradients. The slope from the linear regression is 1.22, which is partially because the range of the modeled gradients is larger than that of the observed ones. Furthermore, the correlation coefficient (CC) is 0.82, which suggests that the two are highly correlated.

The authors also investigated the relationships among gravity gradients, orthometric heights, and the free-air gravity anomalies at every gravity site. Fig. 5 shows the correlations for various pairs. The CCs range from -0.54 to -0.64 [Figs. 5 (a–d)]. In addition, the CC (-0.62) in Fig. 5(a) is very close to the one (-0.64) in Fig. 5(b). Furthermore, the CC (-0.54) in Fig. 5(c) is the same as the one in Fig. 5(d). Therefore, the CCs between the gravity gradient and

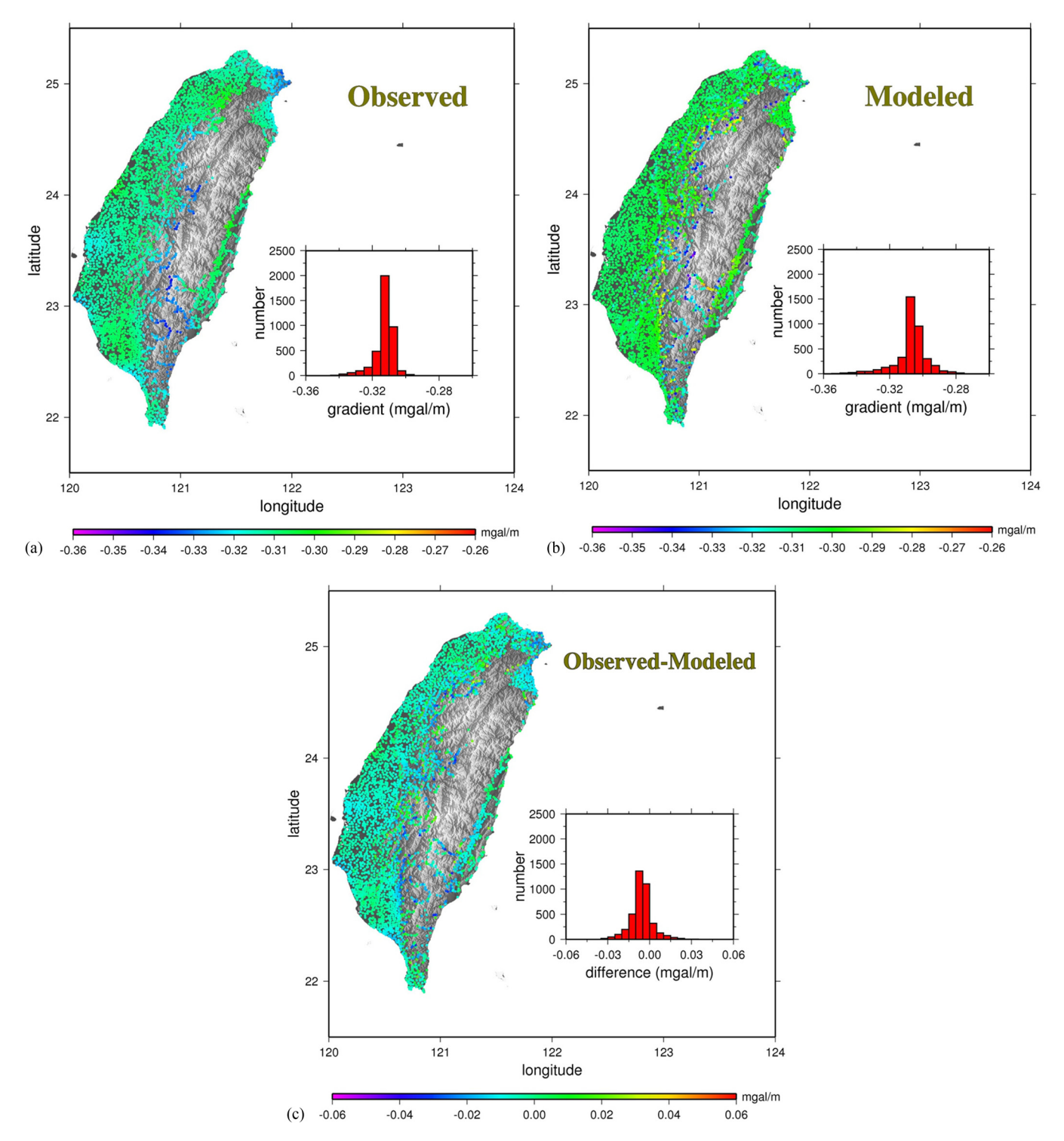


Fig. 3. (Color) (a) Observed gravity gradients; (b) modeled gravity gradients; (c) differences between observed and modeled gravity gradients

orthometric height are almost consistent with the ones between the gravity gradient and the free-air gravity anomaly. These high CCs (absolute values) show that rock densities increase with elevation in Taiwan. This is due to the mountain-building process that led to the presence of denser materials in the highly mountainous areas of Taiwan (Hwang and Hsiao 2003). The CC consistency indicates that both the modeled and observed gravity gradients reflect this density trend.

Although the modeled gravity gradients have more broadly distributed values than the observed ones, they show relatively lower correlations with both orthometric height and the free-air gravity anomaly than the observed gravity gradients. In addition, most observed gravity gradients (absolute values) are larger than 0.3086 gal/m. In particular, the absolute values of gravity gradients tend to increase with orthometric height and the free-air gravity anomaly.

# Using Gravity Gradients for Geoid Modeling: A New Procedure

Using the modeled and observed gravity gradients, the authors proposed a new procedure for geoid modeling. They experimented with three cases of geoid modeling (Table 2): Cases 1–3 use the normal, observed, and modeled gravity gradients, respectively, to reduce the observed gravity values on the ground to the mean sea surface. The geoid modeling strategy in this study is based on the remove-compute-restore (RCR) procedure (Forsberg 1984; Hwang et al. 2007). In this procedure, a geoidal undulation is split into the long-, intermediate-, and short-wave-length parts as follows:

$$N = N_{\text{long}} + N_{\text{int}} + N_{\text{short}} \tag{6}$$

In accordance with this procedure, a gravity anomaly is expressed as

$$\Delta g = \Delta g_{\text{long}} + \Delta g_{\text{int}} + \Delta g_{\text{short}} \tag{7}$$

where  $N_{\rm long}$  and  $\Delta g_{\rm long}$  are the long-wavelength geoid and gravity anomaly, respectively;  $N_{\rm int}$  and  $\Delta g_{\rm int}$  are the intermediate-wavelength geoid and gravity anomaly, respectively; and  $N_{\rm short}$  and  $\Delta g_{\rm short}$  are the short-wavelength geoid and gravity anomaly, respectively. In this study, the values  $\Delta g_{\rm long}$  and  $N_{\rm long}$  are both determined

Table 1. Statistics of Observed and Modeled Gravity Gradients (mgal/m)

Model	Max	Min	Mean	Standard deviation
Observed	-0.2922	-0.3430	-0.3115	0.0057
Modeled	-0.2779	-0.3494	-0.3078	0.0085
Observed-modeled	0.0317	-0.0349	-0.0050	0.0070

from a global geopotential model;  $\Delta g_{\rm short}$  and  $N_{\rm short}$  are derived by the theory of residual terrain model (RTM) (Forsberg 1984) implemented using the fast Fourier transform (FFT) technique; and  $\Delta g_{\rm int}$  represents the remainder after  $\Delta g_{\rm long}$  and  $\Delta g_{\rm short}$  are subtracted from the local gravity observations  $\Delta g$ . The value of  $\Delta g_{\rm int}$  is used to determine  $N_{\rm int}$ . Subsequently,  $N_{\rm long}$  and  $N_{\rm short}$  can be restored to obtain the final geoid.

In this paper, the intermediate-wavelength component,  $N_{\text{int}}$ , is computed from  $\Delta g_{\text{int}}$  by least-squares collocation (LSC) (Moritz 1980)

$$s = C_{sl}(C_{ll} + D)^{-1}l (8)$$

where s and l are vectors of signals and observations, respectively;  $C_{ll}$  is the covariance matrix of l;  $C_{sl}$  is the covariance matrix between s and l; and D is the covariance matrix of the noise contained in vector l, which functions as a filter. In the context of this paper, s, l, and D in Eq. (6) represent a geoidal undulation, gravity anomaly, and the error variance of the gravity anomaly, respectively. The terms  $C_{sl}$  and  $C_{ll}$  denote the covariance matrices for the geoid-gravity anomaly and the gravity anomaly-gravity anomaly, respectively. To construct the previously mentioned covariance matrices, the authors adopted the error anomaly degree variances of the EGM2008 geopotential model for up to 360 degrees (Pavlis et al. 2008, 2012); for higher degrees, the authors adopted the Tscherning-Rapp anomaly degree variance Model 4 (Tscherning and Rapp 1974).

The distribution of the gravity anomalies used for geoid modeling in this paper is only shown in Fig. 2. Because the purpose of this paper is to identify the improvement of geoid modeling by using gravity gradients, the authors use the gravity data associated with Fig. 2 rather than the latest combined gravity data set of Hwang et al. (2014), which is based on earlier land-based [Fig. 1(b)], new land-based (Fig. 2, red dots), shipborne (Fig. 2, green dots), airborne

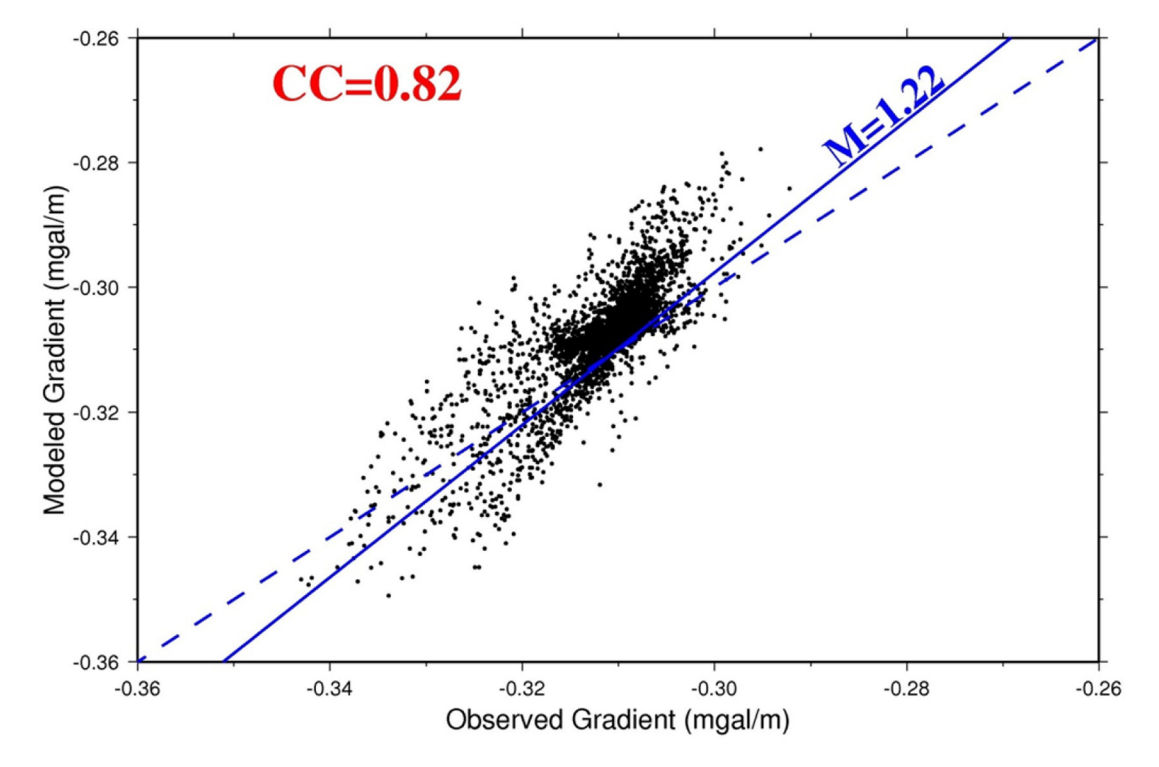
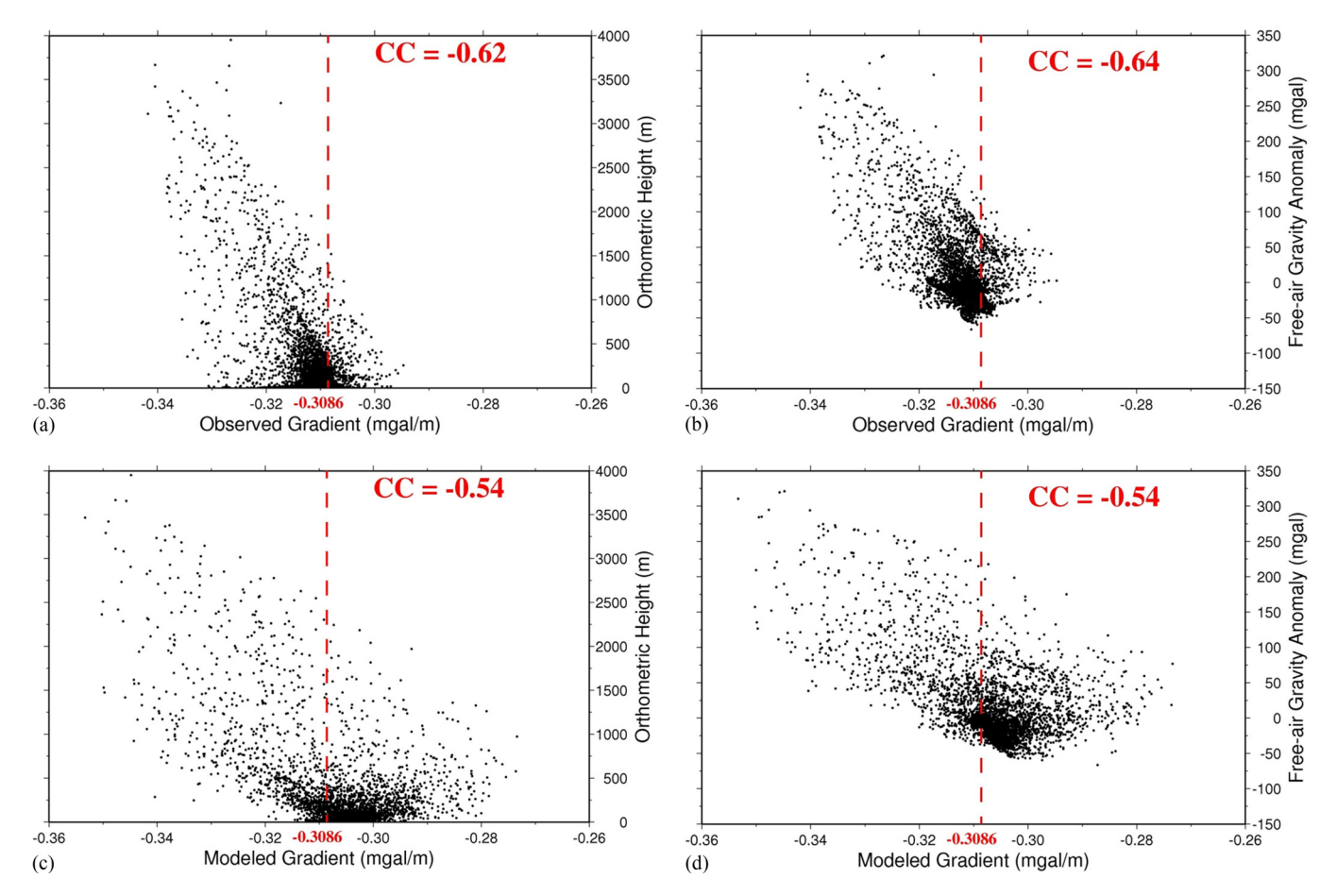


Fig. 4. (Color) Comparison of observed and modeled gravity gradients (Note: CC = CC correlation coefficient; M = CC slope of the linear regression line; and dashed line = best fitting regression line with M = 1.0)



**Fig. 5.** (Color) Relationships among (a) observed gravity gradients and heights, (b) observed gravity gradients and free-air anomalies, (c) modeled gravity gradients and heights, and (d) modeled gravity gradients and free-air anomalies (Note: The dashed red line represents the position of the gravity gradient at -0.3086 mgal/m)

Table 2. Types of Gravity Gradients in the Three Case Models

Case	Type of gravity gradients
1	Normal
2	Observed
3	Modeled

[Fig. 1(c)], and altimeter-derived (Fig. 2, blue dots) gravity data. In Fig. 2, the density of the land-based gravity data (red dots) in flat areas is much higher than that in highly mountainous areas. The earlier land-based gravity data [Fig. 1(b)] of Yen et al. (1990, 1998), which were not used in this paper, were mostly collected in mountainous areas. In addition, to fill the gaps in the ocean and coastal regions, shipborne gravity data (Fig. 2, green dots) from the U.S. National Oceanic and Atmospheric Administration (NOAA) (Hsu et al. 1998) and Taiwan's National Land Surveying and Mapping Center (NLSC) (Hwang et al. 2013) and the gravity field of Sandwell V23.1 (Fig. 2, blue dots) (Sandwell et al. 2014) were used in this paper.

For the long-wavelength geoid and gravity components in Eqs. (6) and (7), the authors adopted a combination of the GOCE-DIR and EGM2008 gravity models extending to 360° and order 360: below 240°, GOCE-DIR coefficients were used; for 241–360°, EGM2008 coefficients were used. This 360° field corresponds to a wavelength of 110 km. Compared with other versions of GOCE solutions, the combined model using GOCE-DIR produces long-

wavelength (model-implied) gravity values that best match the observed gravity values in Taiwan (Wu 2015).

To determine the short-wavelength components in Eqs. (6) and (7), the researchers computed RTM gravity and geoid effects by FFT using three digital elevation models (DEMs) that have three separate spatial resolutions:  $9 \times 9$  arcsec,  $90 \times 90$  arcsec, and  $6 \times 6$  arcmin. The  $6 \times 6$ -arcmin DEM was used as the mean elevation surface (Forsberg 1984) and was used to generate the so-called residual elevations relative to the  $9 \times 9$ - and  $90 \times 90$ -arcsec DEMs. The  $9 \times 9$ - and  $90 \times 90$ -arcsec DEMs were used for the inner and outer zone computations, respectively. The choice of spatial resolution for the three DEMs was based on Hsiao and Hwang (2010).

The previous descriptions in this section focus on the strategy and method of the geoid computation. Here, the authors recommend a new geoid modeling procedure using observed and modeled gravity gradients in two scenarios:

- 1. Geoid modeling if observed gravity gradients are available:
  - Use the observed gradients to reduce ground gravity observations to obtain new free-air gravity anomalies.
  - Use the new gravity anomalies to determine the geoidal undulations.
- 2. Geoid modeling if observed gravity gradients are not available:
  - Use the normal gradient to reduce ground gravity observations to obtain initial free-air gravity anomalies.
  - Combine the initial free-air gravity anomalies and a regular grid of free-air gravity anomalies to compute modeled gravity gradients at the locations of gravity observations.

- Use the modeled gravity gradients to reduce ground gravity observations to obtain new free-air gravity anomalies.
- Use the new gravity anomalies to determine geoidal undulations.

In this study, the researchers computed the geoid undulations on a  $1 \times 1$ -arcmin grid over  $119-123^{\circ}E$  and  $21-26^{\circ}N$ .

#### Results

# Gravity Anomalies from Normal, Observed, and Modeled Gradients

Here, the authors show the impact on the gravity anomaly associated with using gravity gradients other than the normal gradient. Fig. 6 shows gravity results with reductions using the normal gradient (Case 1), observed gradient (Cases 2), and modeled gradient (Case 3) at the gravity sites in Fig. 2 (land values). Figs. 6(a-d) show the gravity anomalies of Case 1 and the gravity anomaly differences between Cases 1 and 2, Cases 1 and 3, and Cases 2 and 3, respectively. The statistics of the differenced gravity anomalies are summarized in Table 3. The results in Fig. 6 and Table 3 show that (1) in certain parts of the highly mountainous areas, the gravity anomaly differences can reach 40-100 mgal, and (2) in most parts of the western plain, the gravity anomaly differences are small (a few mgal). The standard deviations of the gravity anomaly differences for Cases 1-2 and Cases 1-3 are 10.5 and 13.5 mgal, respectively. These two standard deviations are both larger than the standard deviation (7.9 mgal) of Cases 2-3, which use modeled and observed gradients rather than the normal gradient. The large differences in mountainous areas imply large differences in geoidal undulations computed from gravity anomalies based on the normal gradient and modeled/observed gradients.

# Geoid Models from Normal, Observed, and Modeled Gradients

In the previous section, the authors noted the gravity differences caused by using different gravity gradients in the gravity reductions. Here, the authors show the impact of the gravity gradient on the geoid determination by using the three sets of gravity anomalies associated with Fig. 6 and recommend a new procedure for geoid modeling. Using the RCR steps, the authors determined three geoid models using the three sets of gravity anomalies shown in Fig. 6 (Cases 1–3). Fig. 7 shows the geoid model from Case 1. From visual inspections, the geoid models from Cases 2 and 3 are similar to that in Fig. 7, so they are not shown here. The general features of the three geoid models are (1) a distinct, circular low centered at 24°N and 122.8°E and (2) large geoidal height values over the central highly mountainous areas that reach almost 28 m.

The authors then assessed the accuracies of the three geoid models using *observed* geoidal undulations at 63 leveling benchmarks in Taiwan. The researchers' assessments focus on the impact of using different gravity gradients. An observed geoidal undulation at a benchmark is the difference between the ellipsoidal height (at 1-to 2-cm accuracy) and the orthometric height (at a few millimeters of accuracy). The former is obtained from 24-h Global Positioning System (GPS) observations, and the latter is from precision leveling. The authors divided the leveling benchmarks into six routes based on their locations [Fig. 8(a)]. The geographic and topographic features of the six routes are as follows: northern coast (Route 1, 9 points), Longitudinal Valley (Route 6, 10 points), foothills (Route 2, 20 points) to high mountains (Route 3, 6 points), and plains (Route 5,

5 points) to high mountains (Route 4, 13 points). Fig. 8(b) shows the elevations of these leveling benchmarks. The authors divided the benchmarks into two groups, with elevations ranging from 2 to 600 m (<900 m, gentle terrain) and from 933 to 2,500 m (>900 m, rough terrain). There are 48 benchmarks at elevations <900 m and 15 at elevations >900 m. Tables 4 and 5 show the statistics of the differences (in meters) between the observed and modeled geoidal heights at the benchmarks in Fig. 8(a). The differences are grouped according to route (Table 4) and height (Table 5). In Table 4, the geoid model in Case 1 shows geoid discrepancies on the order of several centimeters over moderate terrains (Routes 1, 2, 5, and 6) and 1.2-2.4 decimeters over high mountains (Routes 3 and 4). Two potential reasons for the degraded geoid accuracy over high mountains are (1) poor gravity data coverage over these areas and (2) possible errors in the gravity anomalies caused by the normal gradient. The geoid discrepancies (based on the standard deviations in Tables 4 and 5) in Cases 2 and 3 are close to the discrepancies in Case 1 for Routes 1, 2, 5, and 6 (at the centimeter level). This suggests that gravity anomalies resulting from the normal or observed/modeled gravity gradients will not cause significant geoidal differences over gentle terrain. This conclusion is consistent with the fact that gravity anomalies over gentle terrain are nearly the same, regardless of the gravity gradient used (Fig. 6). However, compared with Case 1, the geoid discrepancies along Route 3 show obvious improvements in both Cases 2 and 3, and the ones along Route 4 show improvements in Case 2. The use of observed (Case 2) and modeled (Case 3) gravity gradients improves the relative geoid accuracy with respect to Case 1 by 17 and 18 cm in Route 3, respectively, and the use of the observed gravity gradients also improves the relative geoid accuracy with respect to Case 1 by 8 cm in Route 4.

Table 5 is consistent with Table 4 in terms of the advantage of using the observed gravity gradients. In Table 5, at elevations < 900 m (gentle terrain), the respective mean and standard deviation of the differences are -0.05 and 0.143 m in Case 1, 0.007 and 0.162 m in Case 2, and 0.009 and 0.149 m in Case 3. At elevations >900 m (rough terrain), the respective mean and standard deviation of the differences are -0.019 and 0.119 m in Case 1, 0.474 and 0.057 m in Case 2, and 0.483 and 0.133 m in Case 3. Compared with the standard deviations over moderate terrain (elevations <900 m), the three geoid modeling statistical results are quite consistent, with an average standard deviation of 14-16 cm. However, in mountainous areas, the results from Case 2 are clearly superior to those from Case 1, based on the smaller standard deviations. The standard deviation of the differences in Case 2 is smaller than that in Case 1 by almost 7 cm, whereas the standard deviation in Case 3 is slightly larger. Case 3 has a slightly worse relative geoid accuracy than Case 1 at elevations >900 m because most leveling benchmarks over this area belong to Route 4, whereas Case 3 provides less improvement to the relative geoid accuracies (Table 4).

Overall, in areas with hills and mountains (Routes 2 and 3), the use of observed (Case 2) or modeled gravity gradients (Case 3) can enhance the relative geoid accuracy. In areas with only high mountains, in which elevations vary from 2,000 to 3,000 m (Route 4), only the use of the observed (Case 2) gravity gradient offers a clear improvement in relative geoid accuracy. The reason the relative geoid accuracy from modeled gravity gradients (Case 3) is not as expected in areas with high mountains may lie in the insufficient gravity data coverage. If dense gravity anomaly data are available for these areas, modeled gravity gradients may further improve the current relative geoid accuracy.

Although the relative geoid accuracy in Case 2 yields better results compared with Cases 1 and 3, as reflected by the smallest

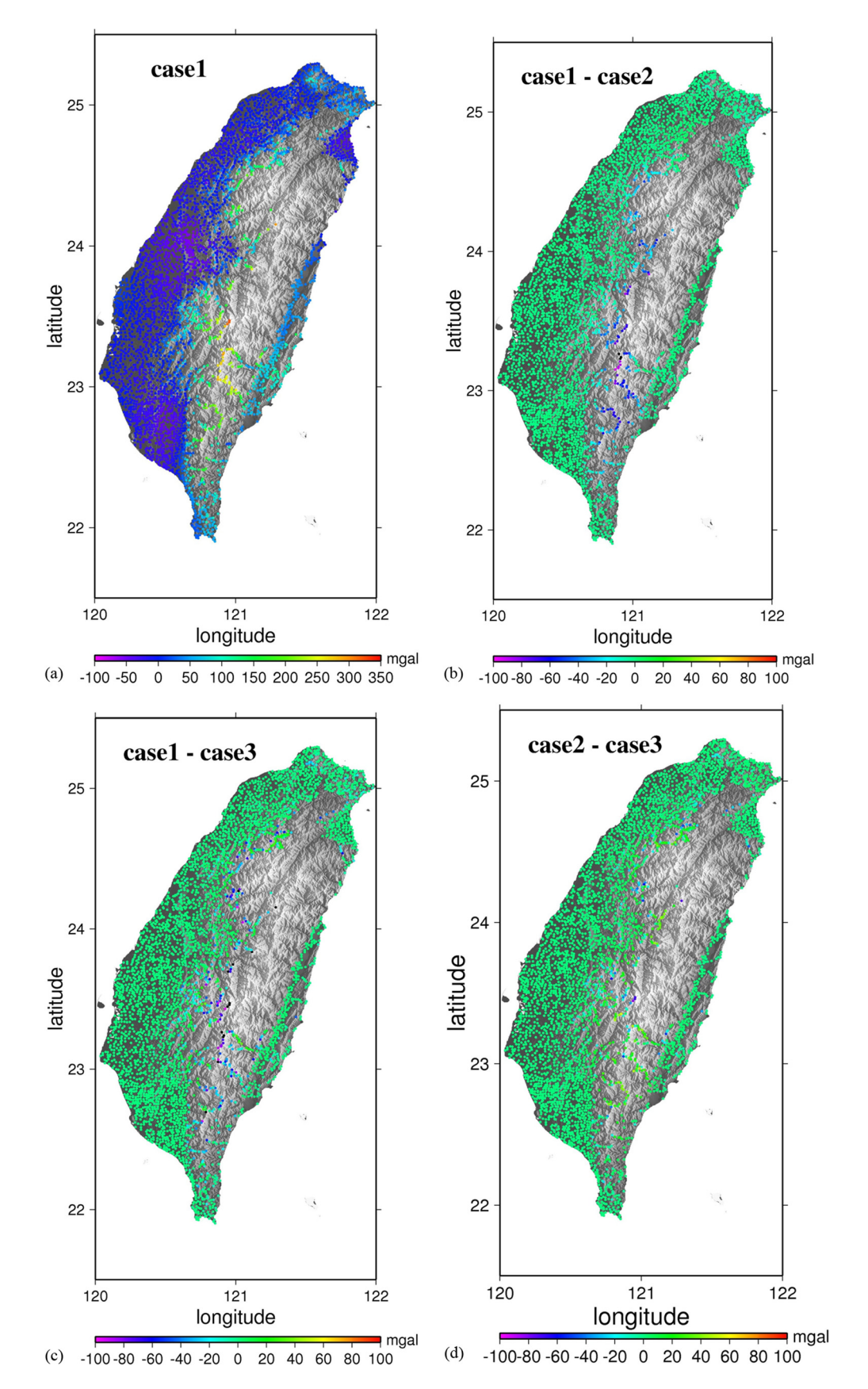


Fig. 6. (Color) (a) Gravity anomalies from Case 1; differences in gravity anomalies from (b) Cases 1 and 2, (c) Cases 1 and 3, and (d) Cases 2 and 3

standard deviations in Tables 4 and 5, the normal gradient (Case 1) still yields the best results, as reflected by the smallest mean values in Tables 4 and 5. The mean values in Cases 2 and 3 are much larger than that in Case 1 due to the large geoidal differences resulting from the use of the gravity anomalies. Figs. 9(a-c) show the differences between the geoidal heights between Cases 1 and 2, Cases 1 and 3, and Cases 2 and 3, respectively. The statistics of the differenced geoidal heights are summarized in Table 6. These differences are most prominent over rough terrain (elevation >900 m) and are mainly caused by the very large gravity anomalies occurring in high mountains in Cases 2 and 3, resulting in geoidal differences of up to 70 cm, as shown in Figs. 9(a and b). In Table 6, at elevations <900 m (gentle terrain), the mean and standard deviation of the differences between Cases 1 and 2 and between Cases 1 and 3 are

**Table 3.** Statistics of the Gravity Anomaly Differences between Cases 1 and 2, Cases 1 and 3, and Cases 2 and 3

Model	Max (mgal)	Min (mgal)	Mean (mgal)	Standard deviation
Cases 1–2	5.2	-116.9	-3.1	10.5
Cases 1-3	37.4	-154.8	-2.2	13.0
Cases 2-3	55.1	-83.6	0.9	7.9

-0.047 and 0.072 m and -0.045 and 0.061 m, respectively. However, at elevations >900 m (rough terrain), the values are much larger than those at elevations <900 m. The mean and standard deviation of the differences between Cases 1 and 2 and between Cases 1 and 3 reach -0.211 and 0.183 m and -0.210 and 0.171 m, respectively. In addition, the geoidal height differences between Cases 2 and 3 are relatively small at elevations both >900 m and < 900 m. Two possible reasons such large mean geoidal differences occur over high mountains between Cases 2 and 3 are (1) the point gravity data are sparse and (2) the observed gravity gradients (absolute values) are relatively large in these areas (Fig. 3). In other words, because the gravity data are sparse, the modeled geoidal undulations are sensitive to changes in gravity values at these data points. One possible method to overcome the large perturbation of modeled geoidal heights is to collect more gravity values and gravity gradients over the high mountains. Again, the authors emphasize that the relative geoidal accuracy is improved by the use of observed gradients over high mountains, and larger mean differences between the modeled and observed geoidal heights over high mountains will be inconsequential when using a hybrid geoid model that combines a gravity-only geoid model (such as any of the models in this paper) with the observed geoidal heights (such as the ones used to assess the gravity-only geoid models).

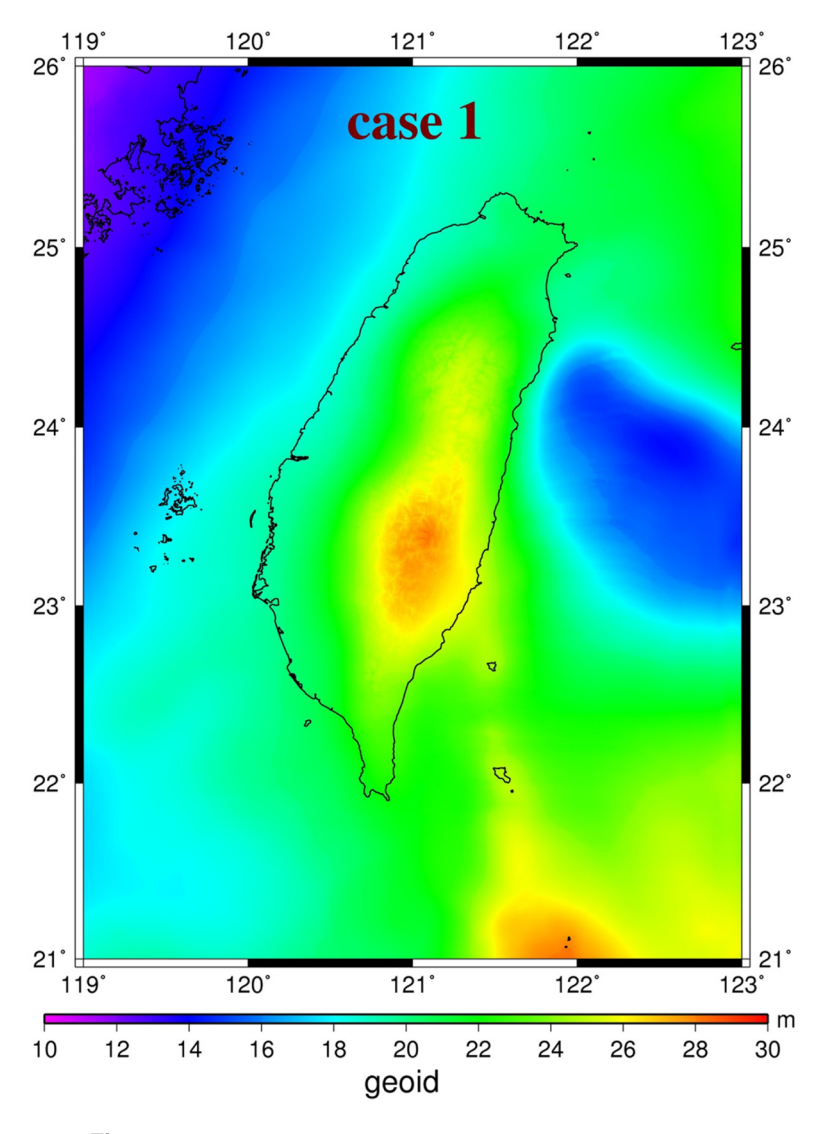


**Fig. 7.** (Color) Geoidal heights using gravity anomalies from Case 1

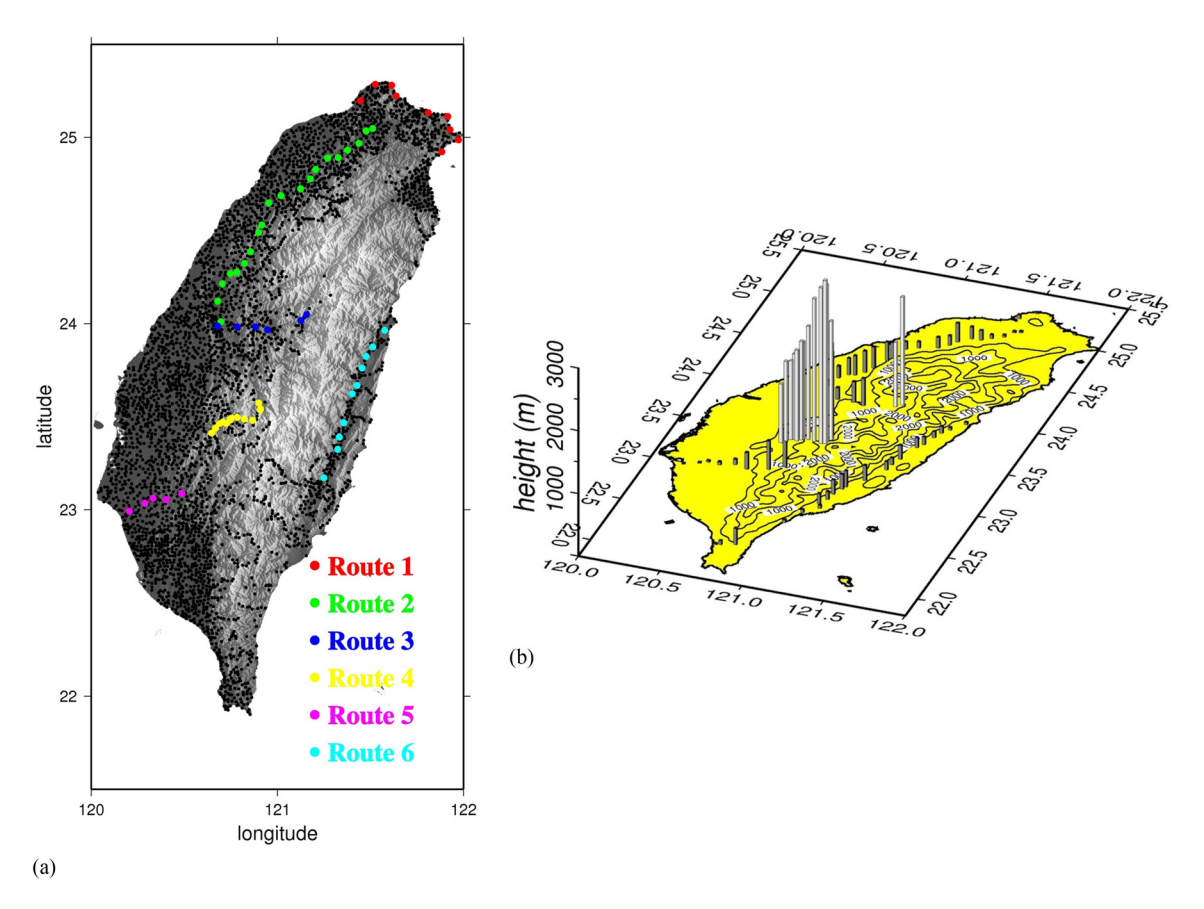


**Fig. 8.** (Color) (a) Distributions of six leveling routes for assessing geoid models, with the new land-based gravity data distribution (black dots) as the background (Fig. 2), and (b) elevations of the leveling benchmarks (Note: White and gray vertical bars correspond to spots in which the elevations are >900 or <900 m, respectively)

**Table 4.** Statistics of Differences between the Observed and Modeled Geoidal Heights at the Test Points (Divided by Route)

Geoid model	Route number	Max (m)	Min (m)	Mean (m)	Standard deviation
Case 1	1	0.060	-0.176	-0.034	0.090
	2	0.174	-0.250	-0.133	0.108
	3	0.437	-0.162	0.138	0.240
	4	0.120	-0.194	-0.004	0.121
	5	0.013	-0.208	-0.068	0.083
	6	0.018	-0.070	-0.017	0.029
Case 2	1	0.073	-0.132	-0.014	0.079
	2	0.194	-0.245	-0.072	0.112
	3	0.593	0.394	0.471	0.076
	4	0.516	0.383	0.461	0.048
	5	0.017	-0.212	-0.073	0.084
	6	0.176	-0.018	0.057	0.055
Case 3	1	0.084	-0.132	-0.017	0.077
	2	0.177	-0.228	-0.065	0.103
	3	0.439	0.273	0.363	0.062
	4	0.675	0.332	0.508	0.124
	5	0.025	-0.206	-0.065	0.085
	6	0.147	0.005	0.072	0.044

Although the gravity anomalies with reduction using observed or modeled gradients cause large geoidal differences in high mountains, the relative accuracies of the geoidal heights using such gradients are improved in these areas. In addition, the differences in geoidal height between Cases 2 and 3 are smaller than those between

**Table 5.** Statistics of Differences between the Observed and Modeled Geoidal Heights at the Test Points (Divided by Height)

Geoid model	Area for statistics $[E(m)]$	Max (m)	Min (m)	Mean (m)	Standard deviation
Case 1	<900	0.437	-0.250	-0.050	0.143
	>900	0.120	-0.194	-0.019	0.119
Case 2	<900	0.459	-0.245	0.007	0.162
	>900	0.593	0.383	0.474	0.057
Case 3	< 900	0.439	-0.228	0.009	0.149
	>900	0.675	0.273	0.483	0.133

other cases; the maximum geoidal difference between Cases 2 and 3 reaches only 30 cm. The geoidal heights in Cases 2 and 3 are more consistent because observed and modeled gradients are both closer to the *true* gravity gradients than the normal gradients.

Although observed gravity gradients can improve geoid accuracy, it is not cost-effective to collect dense gravity gradients to improve geoid accuracy. As a compromise, modeled gravity gradients are an alternative. In conclusion, given sufficient financial resources for geoid modeling in high mountains, measured gravity gradients are preferred. Otherwise, modeled gradients should be used to maximize the local geoid accuracy.

#### Conclusions

This paper shows gravity reductions using observed and modeled gravity gradients to improve relative geoid accuracies over parts

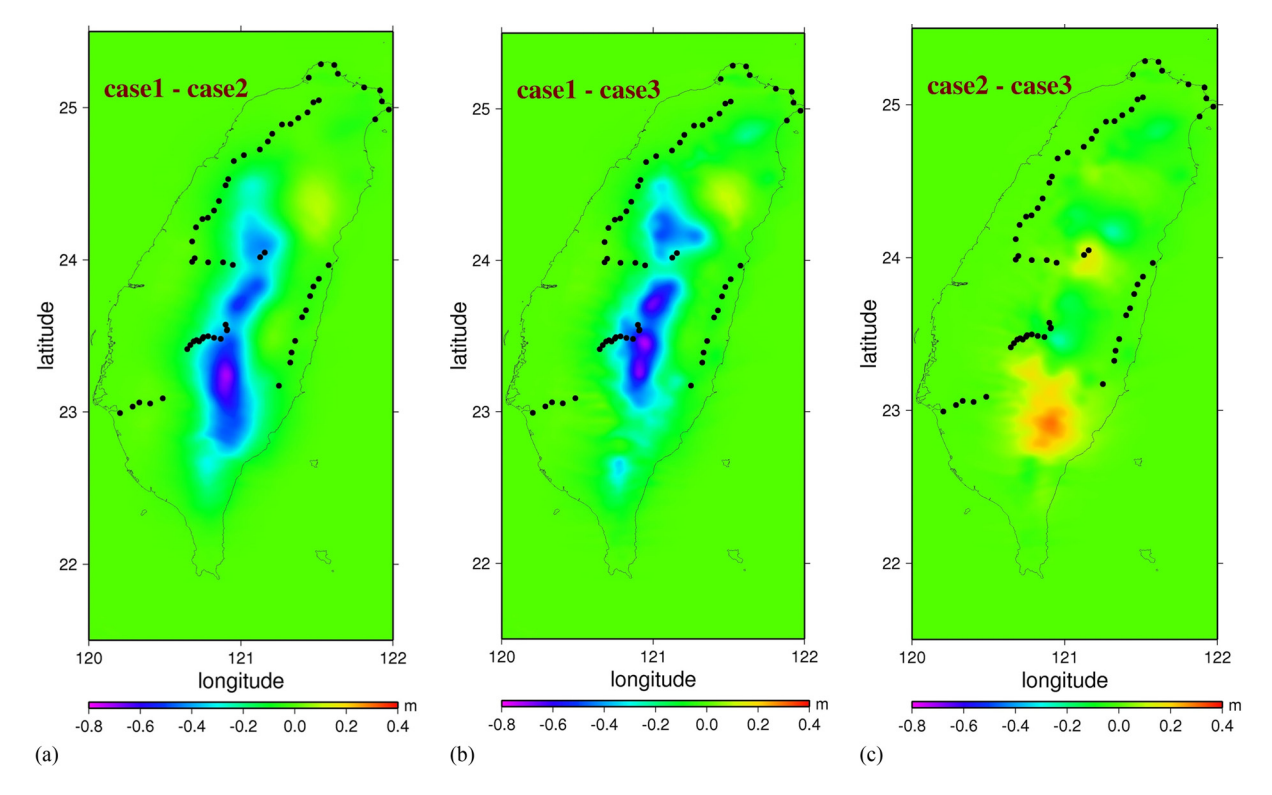


Fig. 9. (Color) Differences in geoidal heights between (a) Cases 1 and 2, (b) Cases 1 and 3, and (c) Cases 2 and 3 [Note: Black dots represent the leveling routes (Fig. 8)]

**Table 6.** Statistics of the Differenced Geoid Undulations between Cases 1 and 2, Cases 1 and 3, and Cases 2 and 3 (Divided by Height)

Geoid model	Area for statistics $[E(m)]$	Max (m)	Min (m)	Mean (m)	Standard deviation
Cases	<900	0.084	-0.052	-0.047	0.072
1-2	>900	0.096	-0.718	-0.211	0.183
Cases	< 900	0.098	-0.657	-0.045	0.061
1-3	>900	0.104	-0.724	-0.210	0.171
Cases	< 900	0.287	-0.160	0.001	0.033
2-3	>900	0.297	-0.233	0.001	0.098

Note: The compared data are only land data.

of mountainous areas in Taiwan. In this paper, the authors do not intend to claim that the use of observed or modeled gradients can offset the need of dense gravity data. Instead, the authors show that such gradients can improve the relative geoid accuracies without adding extra gravity data (Tables 4 and 5). The results imply that one can also collect gravity gradients (in addition to gravity values) during a gravity campaign to add extra observations for an improved geoid. If it is not possible to obtain observed gravity gradients, modeled gravity gradients are an alternative. However, in mountainous areas, gravity data can be sparse due to inaccessible terrain, causing the integration in Eq. (5) to fail to produce reliable modeled gradients. In other words, the accuracy of a modeled gradient at a site can be poor if the gravity data surrounding the site are sparse, thus requiring observation of the gravity gradient.

Next, the authors summarize the key points of this paper:

1. The researchers computed new gravity anomalies using the observed and modeled gravity gradients at more than 4,000

- gravity sites. These gravity anomalies have led to an improved geoid model for Taiwan.
- 2. The use of new gravity anomalies with reductions by observed or modeled gravity gradients can improve the relative geoid accuracy by up to 18 cm.
- 3. If resources are available in a local geoid modeling project over rough terrain, gravity gradients should be measured to produce the best local geoid model.

### **Acknowledgments**

This project is supported by the Ministry of Science and Technology of Taiwan under Grants 104-2221-E-005-078 and 103-2221-E-009-114-MY3.

### References

Forsberg, R. (1984). A study of terrain reductions, density anomalies and geophysical inversion methods in gravity field modelling, Ohio State Univ., Columbus. OH.

Forsberg, R., and Sideris, M. G. (1993). "Geoid computations by the multi-band spherical FFT approach." *Manuscr. Geod.*, 18, 82–90.

Gerald, C. F., and Wheatley, P. O. (1994). Applied numerical analysis, 5th Ed., Addison-Wesley, Reading, MA.

Heiskanen, W. A., and Moritz, H. (1967). *Physical geodesy*, W. H. Freeman, San Francisco.

Hodgson, M. E., and Bresnahan, P. (2004). "Accuracy of airborne Lidar-derived elevation." *Photogramm. Eng. Rem. Sens.*, 70(3), 331–333

Hsiao, Y. S., and Hwang, C. (2010). "Topography-assisted downward continuation of airborne gravity: application to geoid determination in Taiwan." *Terr. Atmos. Ocean. Sci.*, 21(4), 627–637.

- Hsu, S. K., et al. (1998). "New gravity and magnetic anomaly maps in the Taiwan-Luzon Region and their preliminary interpretation." *Terr. Atmos. Ocean. Sci.*, 9, 509–532.
- Hwang, C., et al. (2007). "Geodetic and geophysical results from a Taiwan airborne gravity survey: Data reduction and accuracy assessment." J. Geophys. Res., 112(B4), B04407.
- Hwang, C., et al. (2014). "New free-air and Bouguer gravity fields of Taiwan from multiple platforms and sensors." *Tectonophysics*, 611, 83–93.
- Hwang, C., Cheng, T. C., Cheng, C. C., and Hung, W. C. (2010). "Land subsidence using absolute and relative gravimetry: A case study in central Taiwan." *Surv. Rev.*, 42(315), 27–39.
- Hwang, C., and Hsiao, Y. S. (2003). "Orthometric correction from leveling, gravity, density and elevation data: A case study in Taiwan." J. Geod., 77(5), 279–291.
- Hwang, C., Hsu, H. J., and Huang, C. (2013). "A new geoid model of Taiwan: Applications to hazard mitigation, environmental monitoring and height modernization." *Taiwan J. Geoinform.*, 1(1), 57–81 (in Chinese).
- Hwang, C., Wang, C. G., and Lee, L. H. (2002). "Adjustment of relative gravity measurements using weighted and datum-free constraints." *Comput. Geosci.*, 28(9), 1005–1015.
- Moritz, H. (1980). Advanced physical geodesy, Herbert Wichmann, Karlsruhe, Germany.
- Pavlis, N. K., Holmes, S. A., Kenyon, S. C., and Factor, J. K. (2008). "An earth gravitational model to degree 2160: EGM2008." *Proc.*, 2008 European Geosciences Union General Assembly, European Geosciences Union, Munich, Germany.
- Pavlis, N. K., Holmes, S. A., Kenyon, S. C., and Factor, J. K. (2012). "The development and evaluation of the Earth Gravitational Model 2008 (EGM2008)." J. Geophys. Res., 117(B4), B04406.

- Rapp, R. H., and Pavlis, N. K. (1990). "The development and analysis of geopotential coefficient models to spherical harmonic degree 360." J. Geophys. Res., 95(B13), 21885–21911.
- Rozsa, S., and Toth, G. (2003). "Prediction of vertical gravity gradients using gravity and elevation data." General Assembly of the Int. Association of Geodesy, Springer, Berlin.
- Sandwell, D. T., Müller, R. D., Smith, W. H. F., Garcia, E., and Francis, R. (2014). "New global marine gravity model from CryoSat-2 and Jason-1 reveals buried tectonic structure." *Science*, 346(6205), 65–67.
- Tenzer, R., and Ellmann, A. (2007). "On evaluation of the mean gravity gradient within the topography." General Assembly of the Int. Association of Geodesy/24th General Assembly of the Int. Union of Geodesy and Geophysics, Springer, Berlin.
- Tscherning, C. C., and Rapp, R. H. (1974). Closed covariance expressions for gravity anomalies, geoid undulations, and the deflections of the vertical implied by anomaly degree-variance models, Ohio State Univ., Columbus, OH.
- Vanicek, P., Janak, J., and Huang, J. (2000). "Mean vertical gradient of gravity." IAG Int. Symp. on Gravity, Geoid, and Geodynamics (GGG 2000), Springer, Berlin.
- Völgyesi, L. (2001). "Local geoid determination based on gravity gradients." Acta Geod. Geophys. Hung., 36(2), 153–162.
- Wu, M. L. (2015). Impact of gravity gradient on geoid accuracy, National Chiao Tung Univ., Taiwan (in Chinese).
- Yen, H. Y., Yeh, Y. H., Lin, C. H., Yu, G. K., and Tsai, Y. B. (1990). "Free-air gravity map of Taiwan and its applications." *Terr. Atmos. Ocean. Sci.*, 1, 143–156.
- Yen, H. Y., Yeh, Y. H., and Wu, F. T. (1998). "Two-dimensional crustal structures of Taiwan from gravity data." *Tectonics*, 17(1), 104–111.
- Zhu, L. Z., and Jekeli, C. (2009). "Gravity gradient modeling using gravity and DEM." *J. Geod.*, 83(6), 557–567.